Author/s:
Chen, Z;Russo, SP;Mulvaney, P

Title:
A General Nucleation Model for Semiconductor Nanocrystals

Date:
2024-08-07

Citation:
Chen, Z., Russo, S. P. & Mulvaney, P. (2024). A General Nucleation Model for Semiconductor Nanocrystals. Journal of the American Chemical Society, 146 (31), pp.21600-21611. https://doi.org/10.1021/jacs.4c05361.

Persistent Link:
https://hdl.handle.net/11343/350291

A General Nucleation Model For Semiconductor Nanocrystals

Zifei Chen,[†] Salvy P. Russo,[‡] and Paul Mulvaney[*,†]

†*ARC Centre of Excellence in Exciton Science, School of Chemistry, The University of Melbourne, VIC 3010, Australia.*

‡*ARC Centre of Excellence in Exciton Science, School of Science, RMIT University, Melbourne, 3000, Australia.*

E-mail: mulvaney@unimelb.edu.au

Abstract

We introduce a non-classical model for nanocrystal nucleation in solution which centers on the dynamic interplay of chemical bond breakage and formation, coupled with the desolvation of precursor molecules. Departing from classical theory, our model employs the bond count as the key variable rather than particle size, thereby redefining the role of supersaturation and its role in determining the so-called critical nucleus size. We apply the model to CdSe nanocrystal formation in non-polar solvents and showcase its efficacy in predicting solvent dynamics, precursor characteristics, crystal phase, stoichiometry, "magic number" behavior, and transition states. While the coupled-cluster method is used to determine the bond energy, we show that it is possible to derive reaction pathways by reducing the calculations to algebraic approximations for the nucleation energy. This singular set of bond energy parameters allows nanocrystal nucleation and growth to be conceptualized as a straightforward chemical reaction.

Nucleation theory, semiconductor nanocrystals, critical nucleus, supersaturation, bond energy

Introduction

Nucleation is the critical first step in the formation of a new crystal phase in solution.[1] It holds a central role in understanding nanoparticle (NP) growth and the advancement of our understanding of phase transitions. Nevertheless, experimental investigation of the nucleation process is confronted with formidable challenges. These challenges primarily arise from the need for precise quantification of the size and concentration of nascent, minuscule clusters or nanocrystals (NCs) throughout the growth trajectory.[1–3] Moreover, the absence of size-dependent optical properties during the pre-nucleation phase poses a significant barrier to the identification of a suitable model system for the study of nucleation. Consequently, despite more than a century and a half of extensive research in the field of colloids, the mechanisms that govern the formation of nanoparticles remain contentious.[4–7]

The classical nucleation theories (CNTs) were originally formulated by Becker and Döring in the 1930s[8] and subsequently expanded upon by LaMer and colleagues in the 1950s.[9] These built upon the pioneering work on Ostwald ripening of colloidal solutions, which were developed to explain changes in the size of nanoparticles over time.[8–11] These original models were further improved by Reiss[12] and later refined in the Lifshitz-Slyozov-Wagner (LSW) theory.[13–15] CNT is widely regarded as the foundational model for explaining colloid particle synthesis and relies on the fact that the solubility of a crystal significantly increases as the size decreases, and is quantified by the Gibbs-Thomson equation.[1,3] In this context, continuous crystal growth is expected when the size of the initial crystal embryo surpasses a critical size threshold, referred to as the critical-sized nucleus.

However, numerous studies have shown that CNT falls short in accurately describing various aspects of nanoparticle growth.[16–21] This deficiency stems from the fundamental flaw in CNT, which involves extending bulk-level principles into the prenucleation phase, where a molecular-level understanding is imperative. In the initial stages of nucleation, traditional bulk parameters, e.g. particle size and molar volume become ill-defined. It is also well known that CNT is not satisfied for j-mers when $j = 1$,[22] highlighting the inherent inadequacy

of trying to apply macroscopic material concepts to elucidate molecular-level phenomena. Furthermore, the CNT model neglects surface chemistry, chemical reactions and oxidation state alterations, which often exert significant control over the nucleation process.[23] Although other physical theories such as spinodal decomposition,[24] kinetic theory[25] and quantum-mechanical correction method[26] have been proposed, the field of non-classical nucleation of NPs remains relatively unexplored.

Here we offer an exceptionally precise, atomic-level approach for explaining the complex routes governing the genesis and metamorphosis of NPs. We introduce a unified nucleation model grounded in the dynamic interplay of chemical bond formation/rupture and desolvation. To exemplify the model, we explicitly treat the case of tetrahedral, non-stoichiometric CdSe NCs, one of the most popular nanocrystal systems.

Theory

In the formulation of a nucleation theory, the driving force (ΔG) for nucleation is defined as:

$$\Delta G = G_{\mathrm{NP}} - G_{\mathrm{soln}} \tag{1}$$

By considering those species directly participating in the solvation and desolvation processes, the free energy of the solution, denoted as G_{soln}, and the nanoparticle G_{NP} (comprising both a core and any bound ligands) can be succinctly expressed as the sum of formation or dissociation bond energies using eq. 2:

$$\begin{aligned} \Delta G &= -\left(\underbrace{\sum_{i\in\mathcal{R}} n_{B,i}^{\mathrm{soln}} \epsilon_{B,i}}_{A} + \underbrace{k_B T \ln S_{\mathrm{new}}}_{B} \right) + \underbrace{\sum_{k\in\mathcal{P}} n_{B,k}^{\mathrm{NP}} \epsilon_{B,k}}_{C} \\ &= \underbrace{\left(\sum_{k\in\mathcal{P}} n_{B,k}^{\mathrm{NP}} \epsilon_{B,k} - \sum_{i\in\mathcal{R}} n_{B,i}^{\mathrm{soln}} \epsilon_{B,i} \right)}_{\Delta G^0} - k_B T \ln S_{\mathrm{new}} \end{aligned} \tag{2}$$

where k_B represents the Boltzmann constant and T is the absolute temperature.

The A term on the right-hand side (RHS) of equation 2 represents the estimated Gibbs free energy in the initial solution. This value is derived by summing the bond energies (ϵ_i) of the constituent molecules that are changed during the reaction, and $n_{B,i}^{\text{soln}}$ signifies the number of changed bonds of type i within the direct reacted precursors ($\mathcal{R}$). The B term on the RHS of equation 2 allows for the deviation of the reactant concentration from its equilibrium state. The supersaturation term is defined as

$$\begin{aligned} m[M] + n[E] &\overset{[M_mE_n]^\ddagger}{\rightleftharpoons} [M_mE_n]^* \qquad 1/K_{sp}^{mn} \\ S_{\text{new}} &= \frac{[M]^m[E]^n}{1/K_{sp}^{mn}}. \end{aligned} \tag{3}$$

where the solubility product K_{sp}^{mn} generally depends on the size and composition of the nucleus (i.e. numbers of atoms and type), and follows the Gibbs-Thomson equation

$$K_{sp}([M_mE_n]^*) = K_{sp}([ME]_\infty) \exp[-\Delta G^{mn}/RT]. \tag{4}$$

Here $[M_mE_n]^*$ is the newly formed nucleus characterized by stoichiometry m and n, reached via the transition state $[M_mE_n]^\ddagger$. Note that the energies of $[M_mE_n]^*$ and $[M_mE_n]^\ddagger$ should be supersaturation-independent, given their fixed geometry. The C term in equation 2 denotes the estimated Gibbs free energy associated with the product states. This is calculated by summation of the formation and dissociation bond energies of the newly formed nanoparticles and smaller, molecular by-products.

It is useful to note that in normal nanocrystal synthesis, it is not the active monomers which are normally mixed, but rather stable precursors, which break down into the active monomers. It is imperative to underscore that our model uses the usual chemical precursors as the basic units instead of monomers, whose exact structure is still unknown.[27,28] Our model also makes the fundamental assumption that the standard thermodynamic alteration in free energy is primarily attributed to the molecules or species directly participating in the

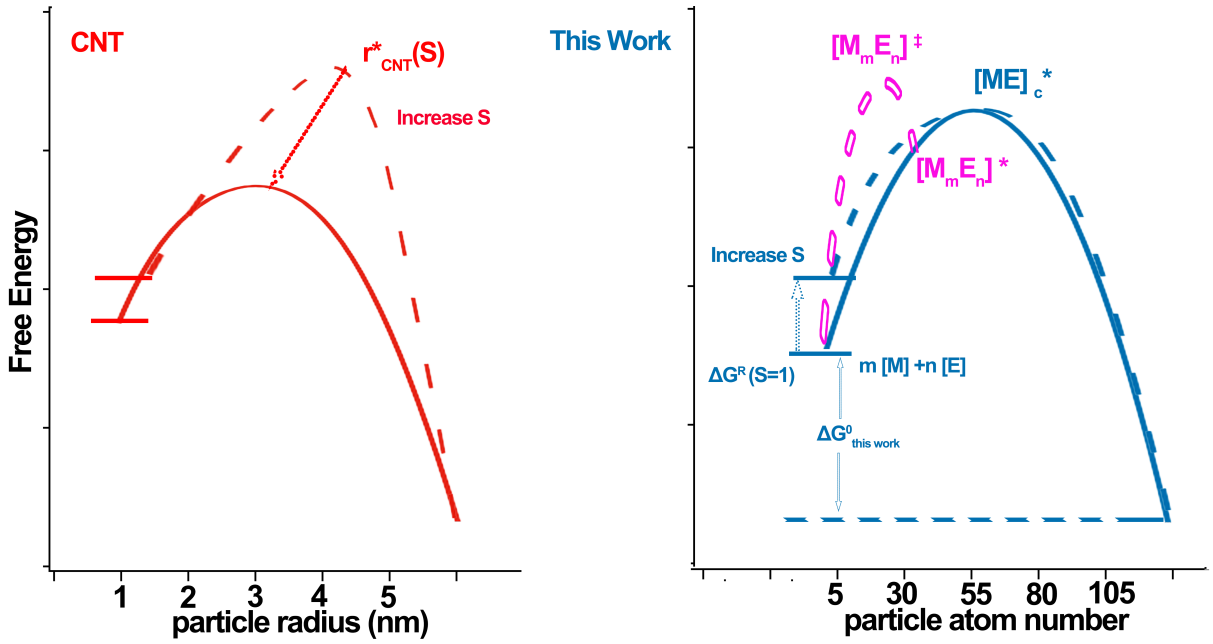

Figure 1: Schematic showing the free energy difference between the CNT model and our model. The blue and red curves represent the free energy changes within the CNT model and this work respectively. The dashed curves indicate the effects of increasing supersaturation. Specifically, the solid blue curve represents the condition when $S_{\text{new}} = 1$. The pink, dashed curve represents the pathway when forming a specific sized nucleus $[M_m E_n]^*$ via the corresponding transition state $[M_m E_n]^{\ddagger}$. The particle size in the CNT model is characterized by a particle radius R, while it is represented by the number of precursor molecules, m and n, in the nascent cluster in the new model.

processes of bond breaking and formation under equilibrium conditions, i.e. $S_{\text{new}} = 1$, and $\Delta G \equiv \Delta G_0$.

As in conventional chemical kinetics we assume that excess precursors or monomers present in the reactant solution do not contribute significantly to the thermodynamic energy of formation of the transition states and critical nuclei, but simply change the energy levels of the reactants, as indicated by the supersaturation term. This obviates the counter-intuitive role of reactant concentration in determining the critical nucleus size, which is a key assumption in CNT theory.

As shown in Figure 1, CNT predicts that the critical size is equal to $\frac{2\sigma\nu}{k_B T \ln S}$, where ν is the molar volume, and σ is the surface tension, indicating that the critical size and nucleation rate change as the supersaturation fluctuates during the reaction. In our model, however, we partition the free energy into the standard component (ΔG^0) and a term accounting for supersaturation. Again, we assume that the energies of the transition state $[M_m E_n]^\ddagger$ and the critical nuclei $[ME]_c^*$ remain constant with respect to supersaturation, reflecting intrinsic properties based on specific chemical reactions. Changes in the rate within our theory result from the elevation of the free energy of the reactants due to increasing supersaturation.

According to CNT, when $S_{\text{CNT}} \leq 1$, nucleation never occurs, as the first term becomes positive-definite, resulting in the entire free energy being positive. In contrast, our model suggests that even if the supersaturation is equal to or slightly less than 1, the bond strength of the forming nanoparticles is likely to be larger than the sum of all the bonds in the precursor molecules, leading to a negative value of the free energy and nucleation.

Interestingly, if we express the CNT free energy as a function of monomer concentration $[M]$ and bulk solubility S_∞ via the following equation:

$$\begin{aligned} \Delta G_{\text{CNT}} &= -\frac{4\pi r^3}{3\nu} k_B T \ln \frac{[M]}{[M]_{\text{ref}}} \frac{[M]_{\text{ref}}}{S_\infty} + 4\pi r^2 \sigma \\ &= \frac{4\pi r^3}{3\nu} k_B T \ln \frac{S_\infty}{[M]_{\text{ref}}} + 4\pi r^2 \sigma - \frac{4\pi r^3}{3\nu} k_B T \ln \frac{[M]}{[M]_{\text{ref}}}, \end{aligned} \tag{5}$$

where $[M]_{\text{ref}}$ is the monomer concentration of a reference state, we can also derive a supersaturation-independent critical radius of $-\frac{2\sigma\nu}{k_B T \ln S_\infty/[M]_{\text{ref}}}$.

Results and Discussions

To achieve generality, we need to include the role of solvent and ligands on the process of nanocrystal nucleation and growth. In the case of a general II-VI non-stoichiometric, metal-rich quantum dot (QD), the chemical formula of the prenucleation cluster may be represented as $[(ME)_x M_y]\, X_{2y} L_{\text{DB}-2y}$. Here, M denotes the metallic element, E signifies the chalcogenide element, x corresponds to the number of stoichiometric components within the cluster, y represents the surplus metal ions which provide the core charge, X stands for the negatively charged ligands (with a requisite count of $2y$ due to charge neutrality constraints), L denotes the charge-neutral, Lewis-base-type ligands and DB signifies the total number of dangling bonds on the bare cluster surface, characterized by the weighted number of surface Cd atoms with less than four coordination. i.e., a three-coordinated Cd surface atom contributes one dangling bond, while a two-coordinated atom contributes 2 dangling bonds. Similar relationships can be obtained for anion-rich clusters. For simplicity, since only coordinating solvents directly participate in the solvation and desolvation process, here we assume the solvent effects are only included in the L-type ligand or coordinating solvents, ignoring the van der Waals interaction from carbon chains.

Stoichiometrically, we expect that a single M^{2+} species will combine with two X ligands, such as acetate, and two more L ligands, such as alkylamines if the reaction is occurring in a coordinating solvent. The simplest form of E is taken to be the corresponding acidic form, e.g., SeH_2, which leads to the following generic nucleation reaction:

$$(x+y)MX_2L_2 + xEH_2 \rightarrow [(ME)_x M_y]X_{2y}L_{DB-2y} + (2x+4y-DB)L + 2xHX.$$

Thus, the free energy of the solution G_{soln} is expressed as:

$$G_{\text{soln}} = (x+y)(n^{\mathcal{R}}_{\text{M-X}}\epsilon^{\mathcal{R}}_{\text{M-X}} + n^{\mathcal{R}}_{\text{M-L}}\epsilon^{\mathcal{R}}_{M-L}) + 2x\epsilon^{\mathcal{R}}_{E-H} + k_B T \ln S_{\text{new}} \tag{6}$$

Here, ϵ denotes the bond energy of the respective species, $\mathcal{R}$ denotes the reactant, and S_{new} signifies the supersaturation of the corresponding metal and chalcogenide species in precursors as defined in eq.3. This expression for G_{soln} is a sum over the changed bonds that directly contribute to, or participate in, the formation of the final cluster structures.

In the final cluster structures, assuming n_{M-E} represents the number of M-E bonds formed within the ultimate cluster, the free energy of the cluster can be formulated as:

$$G_{\text{NP}} = n_{M-E}\epsilon^{\mathcal{P}}_{M-E} + 2y\epsilon^{\mathcal{P}}_{M-X} + (DB-2y)\epsilon^{\mathcal{P}}_{M-L} + 2x\epsilon^{\mathcal{P}}_{X-H} \tag{7}$$

This expression explicitly encapsulates the energy associated with the creation of new M-E bonds, the pre-existing M-X and M-L bonds on the nanoparticle surface, $\mathcal{P}$ represents the chemical products, which depend upon the surface chemistry, and must also include the formation of new, small X-H molecules. The net effect of the driving force arises from the difference in the energy to break the original precursor bonds, the desolvation of precursor molecules, the establishment of new M-E bonds in the emerging clusters, and the formation of new bonds for small, acidic by-products. Since the determination of n_{M-E} in equation 7 is not straightforward for the general case, we will delve into tetrahedral case to illustrate this more clearly.

Tetrahedral CdSe Nanocrystals

In the case of CdSe, solution phase nucleation and growth is normally carried out using the hot injection process and results in wurtzite or zincblende structured clusters, which subsequently grow into monocrystalline and close-to-monodisperse, semiconductor NCs or QDs.

We will denote the initial nuclei that form during nucleation as "clusters". Furthermore, it has been found by numerous investigations that there are often preferred nuclei numbers present during the formation of clusters, so-called "magic sized" clusters. Hence, tetrahedral nanocrystals are the end product of nucleation and growth of tetrahedral, magic-sized clusters (MSCs).[29,30] We choose tetrahedral clusters because the nucleation number follows a simple geometric form and in addition, they possess a unique surface characteristic: the presence of only one type of atom on all surfaces.

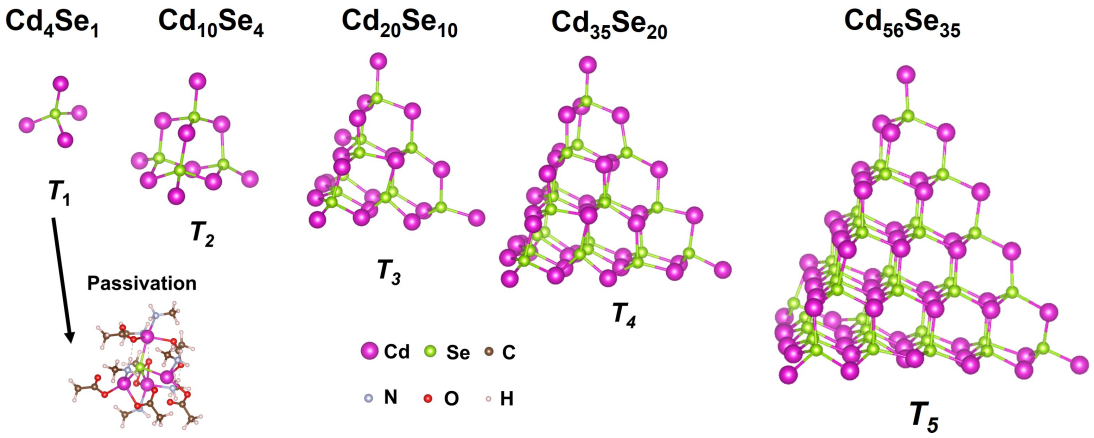

Figure 2: Structures of tetrahedral zincblende CdSe MSCs coated with carboxylate and alkylamine ligands.

Figure 2 provides insight into the structural characteristics of tetrahedral (zincblende) CdSe clusters. These clusters exhibit a core configuration featuring pyramidal structures with exposed, Cd-rich {111} facets.[31–33] Their general stoichiometry can be represented as $\mathrm{Cd}_{\frac{(n+1)(n+2)(n+3)}{6}}\mathrm{Se}_{\frac{n(n+1)(n+2)}{6}}$. Note that this structure automatically demands the inclusion of X-type ligands to balance the excess core charge. Each additional Cd^{2+} ion introduces two positive charges, thus requiring $(n+1)(n+2)$ X-type ligands. Moreover, to minimize the number of dangling bonds, Cd atoms favor an sp^3 tetrahedral geometry, bonding to 3, 2, and 1 ligands at the vertices, edges, and facets, respectively. Consequently, an additional $(n+1)(n+2)$ L-type ligands are needed, resulting in the final chemical formula for a tetrahedral cluster, $T_n = \mathrm{Cd}_{\frac{(n+1)(n+2)(n+3)}{6}}\mathrm{Se}_{\frac{n(n+1)(n+2)}{6}}X_{(n+1)(n+2)}L_{(n+1)(n+2)}$. This formulation

clearly indicates that the nucleation of covalently bonded MSCs is fundamentally different to the hard sphere model which simply postulates monomers as the basic unit.[34] Clearly, the stoichiometry of clusters cannot be completely arbitrary and energy minimization based on conservation of charge and stoichiometry can help to identify the most probable pathways to nucleation.

Notably, the entire cluster stoichiometry changes when transitioning from one layer to the next. For instance, moving from the simplest tetrahedral nucleus T_1 (Cd_4Se_1) to T_2 ($Cd_{10}Se_4$) involves the addition of six Cd atoms and three Se atoms, while progressing from T_2 to T_3 ($Cd_{20}Se_{10}$) results in a gain of ten Cd atoms and six Se atoms. It is evident that the conventional approach, which treats the CdSe monomer as the basic unit of growth is not suitable.[30,34] Moreover, Figure 2 also illustrates the importance of ligand number, where we have employed $CH_3CO_2^-$ and CH_3NH_2 as model ligands to represent the alkylcarboxylate acid and alkylamine molecules used in practice.

Solvent Effect

When utilizing the commonly employed cadmium oleate/acetate molecule as the cadmium precursor in either a non-coordinating solvent such as octadecene (ODE) or alkylamine solution, the cadmium ions will associate with the negatively charged acetate/oleate groups first, and then there will be additional coordinating N atoms which bind to the central cadmium ions if reaction occurs in alkylamine rich solvents. This leads to the formation of a well-solvated $Cd(acetate)_2$ or $Cd(acetate)_2(amine)_2$ complex within the ODE or amine solution, respectively. Upon introducing the selenium precursor, such as SeH_2 in the simplest case, four Cd precursor molecules react with one SeH_2 to yield T_1, Cd_4Se_1. This reaction entails the breaking of a certain number of Cd-O bonds in the original cadmium precursor, along with the cleavage of two Se-H bonds, resulting in the formation of four Cd-Se bonds and two acetic acid molecules with newly formed O-H bonds. We expect that only six amine ligands will remain attached to the final cluster. Consequently, two amines must detach from

the initial cadmium precursor and these are liberated, reflecting the solvation and desolvation dynamics during this reaction.

Hence we write for the reaction of $Cd(acetate)_2$ with SeH_2:

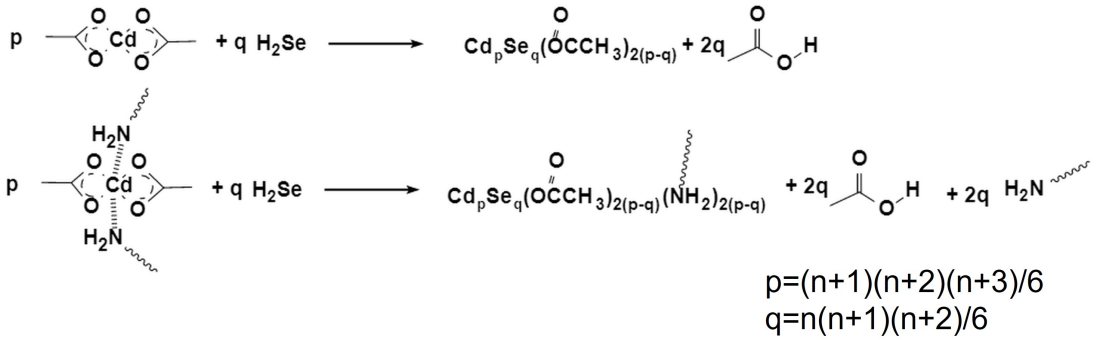

Then, utilizing equations 1, 6, and 7, and after incorporating the composition of tetrahedral clusters, we can deduce the driving force for nucleation for in the non-coordinating solvent case to be:

$$\begin{aligned}\Delta G_{\text{non-coordinating}}(n) &= \left[4n_{\text{Se}}\epsilon^{\mathcal{P}}_{Cd-Se} + n_X\epsilon^{\mathcal{P}}_{Cd-O} + 2n_{Se}\epsilon^{\mathcal{P}}_{O-H}\right] \\ &\quad - \left[n_{Cd}n^{\mathcal{R}}_{\text{Cd-O}}\epsilon^{\mathcal{R}}_{\text{Cd-O}} + 2n_{\text{Se}}\epsilon^{\mathcal{R}}_{\text{Se-H}} + k_BT\ln S_{\text{new}}\right] \\ &= \left[\frac{n(n+1)(n+2)}{6}(4\epsilon^{\mathcal{P}}_{Cd-Se} + 2\epsilon^{\mathcal{P}}_{O-H}) + (n+1)(n+2)\epsilon^{\mathcal{P}}_{Cd-O}\right] \\ &\quad - \left[\frac{(n+1)(n+2)(n+3)}{6} \times 4\epsilon^{\mathcal{R}}_{Cd-O} + 2 \times \frac{n(n+1)(n+2)}{6}\epsilon^{\mathcal{R}}_{Se-H} + \text{S.T.}\right],\end{aligned} \tag{8}$$

where S.T. represents the supersaturation terms. The standard thermodynamic contribution ΔG^0, on the other hand, arises solely from the disparity in free energy between the initial, solvated reactants and the newly formed clusters along with any small product molecules in the equilibrium state, i.e. it is independent of the monomer or precursor concentration. To accomplish this, we initially set the supersaturation term to zero as the standard condition in the following discussions. The bond energies in this study are then calculated with the domain-based pair natural orbital coupled-cluster method (DLPNO-CCSD(T))[35] and are

listed in Table 2.

In the case of coordinating solvents, one of the most prominent distinctions between these two solvent types is that coordinating solvents directly interact with the metal ions to form cation precursors, influencing the composition of the final nanoparticles. For instance, in an alkylamine solution, apart from the two carboxylate ligands, two additional alkylamine molecules will bind to the cadmium ions, altering the driving force in the amine solution to

$$\begin{aligned}\Delta G^{0}_{\text{coordinating}}(n) &= \left[4n_{\text{Se}}\epsilon^{\mathcal{P}}_{Cd-Se} + n_X\epsilon^{\mathcal{P}}_{Cd-O} + n_L\epsilon^{\mathcal{P}}_{Cd-N} + 2n_{Se}\epsilon^{\mathcal{P}}_{O-H}\right] \\ &\quad - \left[n_{Cd}(n^{\mathcal{R}}_{\text{Cd-O}}\epsilon^{\mathcal{R}}_{\text{Cd-O}} + n^{\mathcal{R}}_{\text{Cd-N}}\epsilon_{\text{Cd-N}}) + 2n_{Se}\epsilon^{\mathcal{R}}_{Se-H}\right] \\ &= \left[\frac{n(n+1)(n+2)}{6}(4\epsilon^{\mathcal{P}}_{Cd-Se} + 2\epsilon^{\mathcal{P}}_{O-H}) + (n+1)(n+2)(\epsilon^{\mathcal{P}}_{Cd-O} + \epsilon^{\mathcal{P}}_{Cd-N})\right] \\ &\quad - \left[\frac{(n+1)(n+2)(n+3)}{6}(3\epsilon^{\mathcal{R}}_{Cd-O} + 2\epsilon^{\mathcal{R}}_{Cd-N}) + 2 \times \frac{n(n+1)(n+2)}{6}\epsilon^{\mathcal{R}}_{Se-H}\right]\end{aligned} \tag{9}$$

Comparing equation 8 and equation 9 we see that the latter incorporates the energy associated with Cd-N bonds in the precursor molecules, as well as those in the resultant nanoparticles. It is worth noting that the existing Cd-O bonds in the precursor molecules are partially replaced by amines, resulting in the formation of hydrogen bonds. In this context, an average value of three is used to represent the number of Cd-O bonds.

Figure 3 (a) depicts the standard free energy landscape using our model for tetrahedral CdSe MSCs adorned with oleate ligands in a non-coordinating solution, such as ODE, and in a coordinating alkylamine solution as a function of the number of layers, n. Evidently, the free energy experiences an initial upsurge during the early stages (corresponding to layer numbers less than five). At this juncture, the energy required to form new Cd-Se bonds is insufficient to offset the energy consumed in breaking the Cd-O bonds within the original precursor molecules. This observation aligns with the findings of the CNT, which postulates that smaller clusters/NCs have higher energy. The barrier to nucleation is self-evident from this formulation: it is the difference in energy between solvated precursors and the energy

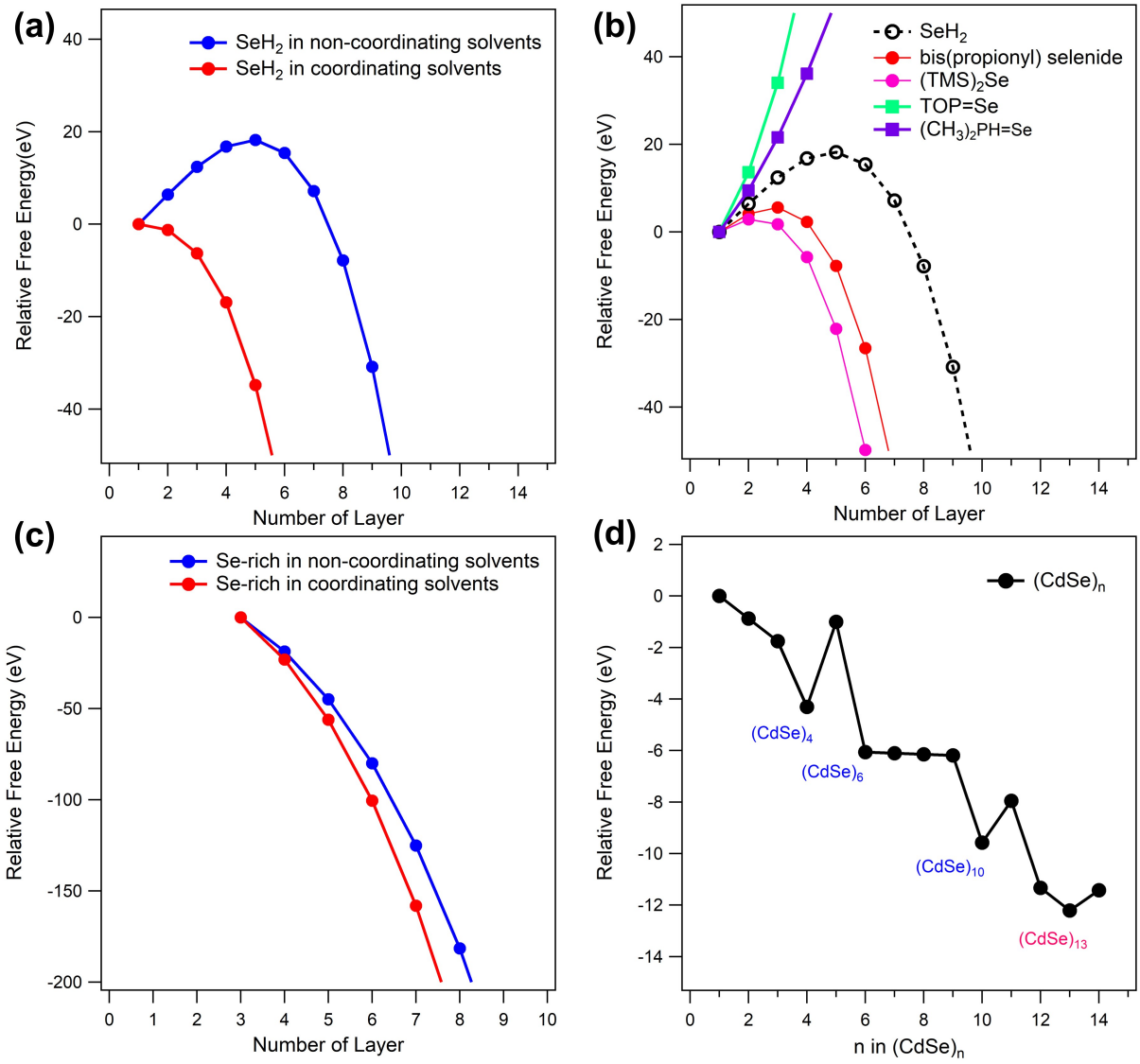

Figure 3: (a) Predicted free energy landscape during formation of Cd-rich zincblende CdSe MSCs using Cd acetate and SeH_2 as the precursors in both non-coordinating and alkylamine-based coordinating solvents.(b) Predicted free energy landscape during formation of Cd-rich tetrahedral CdSe MSCs in the presence of different Se precursors. (c) Predicted free energy landscape during formation of Se-rich, zincblende, CdSe MSCs using Cd acetate, butaneselenol and SeH_2 as precursors.(d) Predicted free energy landscape of stoichiometric $(CdSe)_n$ with amine ligands.

recovered from formation of the nascent cluster.

However, once the particle size attains a critical layer count, n_{crit}, (in this case, $n_{\text{crit}} \approx 5$), the free energy change associated with the formation of the nascent cluster goes through a maximum and, for $n > 8$ the overall free energy change becomes negative. Consequently, the free energy continues to decrease, signifying that a spontaneous process becomes attainable after surpassing a "critical value of n." This graph demonstrates that although the bulk free energy change for formation of CdSe < 0, the nucleation and early growth pass through a series of high energy clusters. This outcome suggests that the newly established bond is more robust than the bond present in the original solution after a certain size, which aligns with the large size limit of CNT.

What is more satisfying about this approach is there is no need to arbitrarily invoke the formation of a surface nor to determine an average equivalent radius to use in estimating the critical nucleus size. Nucleation occurs in a size regime where a molecular approach is more intuitive and more chemically precise. It is also amenable to computational evaluation using quantum-mechanical methods such as coupled-cluster or density functional theory (DFT).

Transitioning from a non-coordinating solvent to a coordinating one e.g. an alkylamine rich solution, leads to a significant reduction in the reaction barrier, suggesting that the formation of nanoparticles is more favorable in amine solutions than in non-coordinating solvents, i.e. binding of the amine to the cluster compensates for the increase in bond energy of the amine ligated precursor. This is consistent with the experimental fact that alkylamines are used to make smaller QDs.[36]

In our model, the critical size highlights the pivotal role of the interaction between bond strengths before and after the reaction in driving nucleation. Initially, the newly formed bonds lack the strength to stabilize the entire cluster system. However, as more bonds form nonlinearly, the molar formation energy of the nanocrystals becomes favorable. This contrasts fundamentally with the CNT perspective, which attributes the driving force to differences in solubility. More discussions about the spontaneous nucleation condition can

be found in the SI.

Precursor Effect

The precursor molecules have been shown to play a crucial role in the synthesis of QDs.[37,38] Figure 3(b) illustrates how the choice of precursor greatly influences the formation of NPs by our model, particularly those involving selenium. The energy landscapes during nucleation in the presence of several common selenium precursors: SeH_2, bis(propionyl)selenide,[29,30,39] $Se(TMS)_2$,[32] $Se{=}P(CH_3)_3$ to represent trioctylphosphine selenide (TOP=Se) and $Se{=}PH(CH_3)_2$ to represent dioctylphosphine selenide (DOP=Se) in non-coordinating solvents are chosen for demonstration. The corresponding reactions are proposed to be

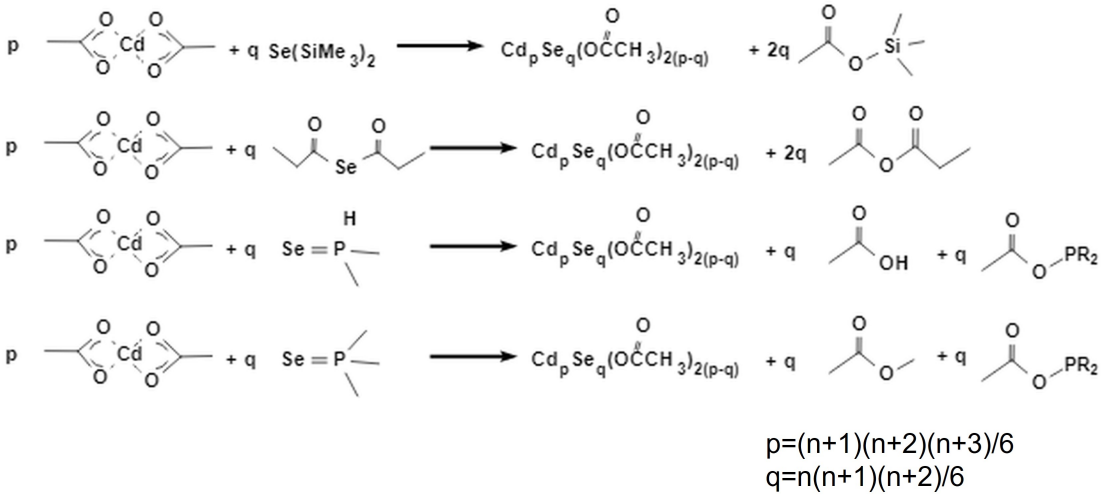

$Se(TMS)_2$ and bis(propionyl)selenide are predicted to exhibit a greater propensity for generating critical nuclei of tetrahedral clusters, compared to SeH_2, which aligns with findings from the Owen and Norris groups, who utilized these precursors to synthesize small CdSe clusters.[30,32] Conversely, the introduction of $Se{=}P(CH_3)_3$ results in significant increase in free energy due to the disruption of the P-C bond. Similarly, when employing $Se{=}PH(CH_3)_2$, a considerable reaction barrier is observed, with a critical layer number $n_{\mathrm{crit}} = 27$. This prediction indicates that the formation of tetrahedral NCs becomes exceedingly challenging when using TOP=Se or secondary phosphine precursors, while other cluster morphologies

may still be possible.

This showcases our model's ability to differentiate various chemistries through the manipulation of precursor reactivity, a factor neglected in conventional CNT.

Stoichiometry Effect

The standard CdSe quantum dots are typically enriched with cadmium due to the sole availability of carboxylate surface ligands in the synthetic system. However, under certain circumstances, it is also possible to achieve a selenium-rich crystal.[40,41] By simply exchanging the Cd and Se atom numbers, our model can cater for the formation of Se rich tetrahedral CdSe QDs where the surface is comprised of solely selenium anions.

Due to the surplus of selenium anions, the core of these QDs becomes negatively charged, and it can be challenging to find suitable positive counter ions other than metal ions to stabilize these clusters. One approach to address this issue and obtain a perfect Se-rich QD is to use selenols (RSe^-) or R_2PSe^- to replace some of the surface selenium atoms, thereby rendering the entire particle charge-neutral. This is analogous to the effect of using R^+ or PR_2^+ ligands as positive counter ions, except that the selenium anions in the core will, to some extent, originate from the ligand.

Selenols can serve as an example of how selenium-rich tetrahedral particles can be represented

$$\left[\mathrm{Cd}_{\frac{n(n+1)(n+2)}{6}}\mathrm{Se}_{\frac{(n+1)(n+2)(n-3)}{6}}\right]\left(\mathrm{SeR}^1\right)_{(n+1)(n+2)}$$

Note that if an alkylamine is present, this expression remains unchanged since there are no available surface Cd sites to bind with the amine. We can then express the reactions to form selenium rich nuclei as

The standard free energy change for the formation of Se rich clusters may be written as

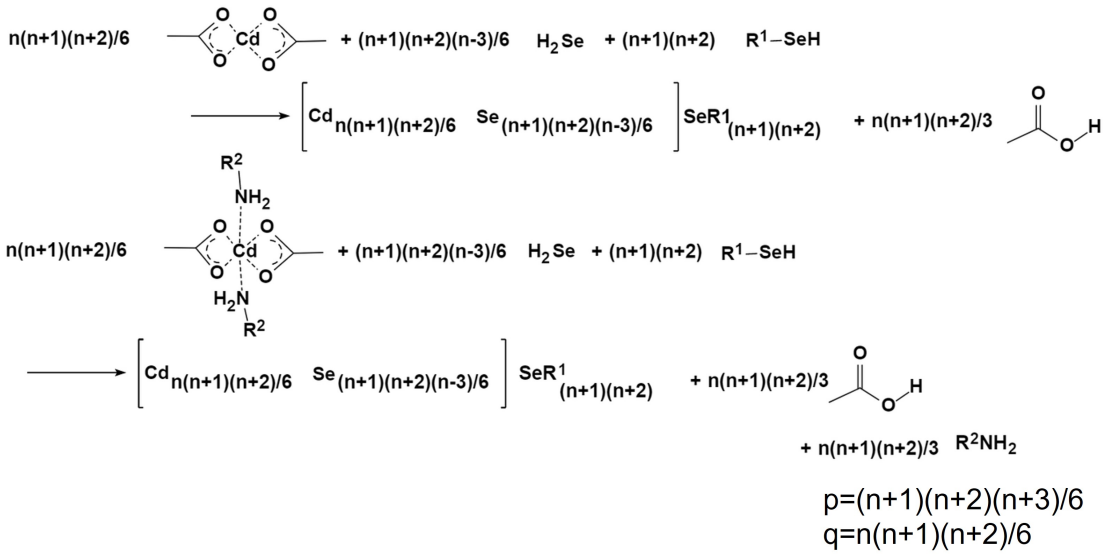

follows:

$$\Delta G^{0}_{\text{Se-rich}}(n) = \begin{cases} \left[4n_{\text{Cd}}\epsilon^{\mathcal{P}}_{Cd-Se} + \frac{1}{3}n(n+1)(n+2)\epsilon^{\mathcal{P}}_{O-H}\right] \\ \quad - \left[n_{\text{Cd}}4\epsilon^{\mathcal{R}}_{Cd-O} + 2\frac{(n+1)(n+2)(n-3)}{6}\epsilon^{SeH_2}_{Se-H} + (n+1)(n+2)\epsilon^{RSeH}_{Se-H}\right], \\ \text{(in non-coordinating solvents)} \\ \left[4n_{\text{Cd}}\epsilon^{\mathcal{P}}_{Cd-Se} + \frac{1}{3}n(n+1)(n+2)\epsilon^{\mathcal{P}}_{O-H}\right] \\ \quad - \left[n_{\text{Cd}}(3\epsilon^{\mathcal{R}}_{Cd-O} + 2\epsilon^{\mathcal{R}}_{Cd-N}) + 2\frac{(n+1)(n+2)(n-3)}{6}\epsilon^{SeH_2}_{Se-H}\right. \\ \quad \left. +(n+1)(n+2)\epsilon^{RSeH}_{Se-H}\right], \text{ (in amine solvents)} \end{cases} \tag{10}$$

where $n_{\text{Cd}} = \frac{n(n+1)(n+2)}{6}$, and $n \geq 3$.

Figure 3 (c) illustrates the free energy change as a function of the number of layers, n, in the formation of selenium-rich tetrahedral MSCs in both non-coordinating and amine-rich solutions. When n $<$ 3, there is no surplus of positively charged ligands to offset the negative core charge without adding cations. One possible solution is to introduce $[\text{N}(\text{CH}_3)_4]^+$ cations to compensate for this effect.[42] On the other hand, when n $>$ 3, the free energy consistently remains negative when using selenol as the reactant, indicating

the potential to create selenium-rich particles using selenol as the precursor. Additionally, the decrease in free energy in the amine solution is greater than that in non-coordinating solvents, which aligns with our previous discussion regarding cadmium-rich results. Notably, this process does not entail the rupture and establishment of Se-R bonds. Consequently, the R ligand originates directly from the precursor molecules along with the selenium atoms.

Trioctylphosphine selenide is a common precursor used in nanocrystal synthesis. Opting for Se=TOP as the precursor would likely result in the removal of one alkyl group from the P atom, leaving the PR_2 group with a single positive charge. Consequently, we anticipate that $Se{=}PHR_2$ would exhibit higher reactivity compared to Se=TOP. It is worth noting that alternative methods, such as L to Z-type ligand exchange, could also generate a selenium-enriched surface by replacing the entire CdX_2 group with an L-type ligand. However, such processes may lead to surface etching and may not maintain pristine Se-facets.

Magic Number Behavior

We now proceed to examine the $(CdSe)_n$ family with a focus on a predetermined bond number and dangling bond configuration for cases where n is less than 14, as outlined in Table 1. The variation in free energy with respect to the size of $(CdSe)_n$ is depicted in Figure 3 (d), using $Cd(O_2CCH_3)_2(CH_3NH_2)_2$ and SeH_2 as precursors. Interestingly, the free energy of each size displays distinctive, oscillatory patterns instead of following a monotonic trend. Notably, $(CdSe)_{13}$ exhibits a significantly lower free energy of formation compared to other sizes. This is an exciting outcome of the model, since precisely this "magic sized cluster" has been identified in experiments.[43] However, it is crucial to highlight that the determination of this particular "magic number" is contingent on the chosen MSC isomers, as well as ligand choice and necessitates further investigation.[44,45]

Table 1: Numbers of Cd-Se bonds and dangling bonds (DB) in the newly formed, stoichiometric $(CdSe)_n$ magic-sized clusters.

n	1	2	3	4	5	6	7	8	9	10	11	12	13	14
$n_{Cd\text{-}Se}$	1	4	7	12	10	18	20	22	24	30	31	36	39	41
n_{DB}	3	4	5	4	10	6	8	10	12	10	12	12	13	14

Transition State Kinetics

The above model enables realistic determination of the free energy of formation of critical clusters involved in nanocrystal synthesis. However, another core aspect of particle synthesis is predicting the kinetics of the nucleation process in the equilibrium condition, i.e. $S_{\text{new}} = 1$. Navigating this pathway can be highly complex, necessitating the accurate conjecture of a transition state (TS) structure, i.e. we need to model not just the energy of the various clusters as a function of n but also to predict how successive layers will form. One plausible TS envisions a series of triangular adlayers.[34] In this particular scenario, we hypothesize that the transition state involves the partial removal of carboxylate ligands from the reaction surface, followed by the addition of Se and Cd atoms, culminating in ligand re-passivation to fully saturate the emerging CdSe "island."

As shown in figure 4 (a), the easiest scenario to imagine is one where the triangular layer on top matches the middle layer of the entire tetrahedron, represented as int$(n/2)$, where "int" is a function to round a number down to the nearest integer (more precisely, if $n/2 = 3.7$, a number of 3 will be taken instead of 4). For instance, in the 4th layer, the transition state involves addition of a triangle identical to the one in the 2nd layer. Similarly, in the 15th layer, the TS entails adding a triangle that is the same as the one in the 7th layer. Since, for each layer, the number of Cd atoms exceeds the number of Se atoms, the addition of the next layer fails to completely cover the entire, pre-existing Cd surface. This process can be expressed as

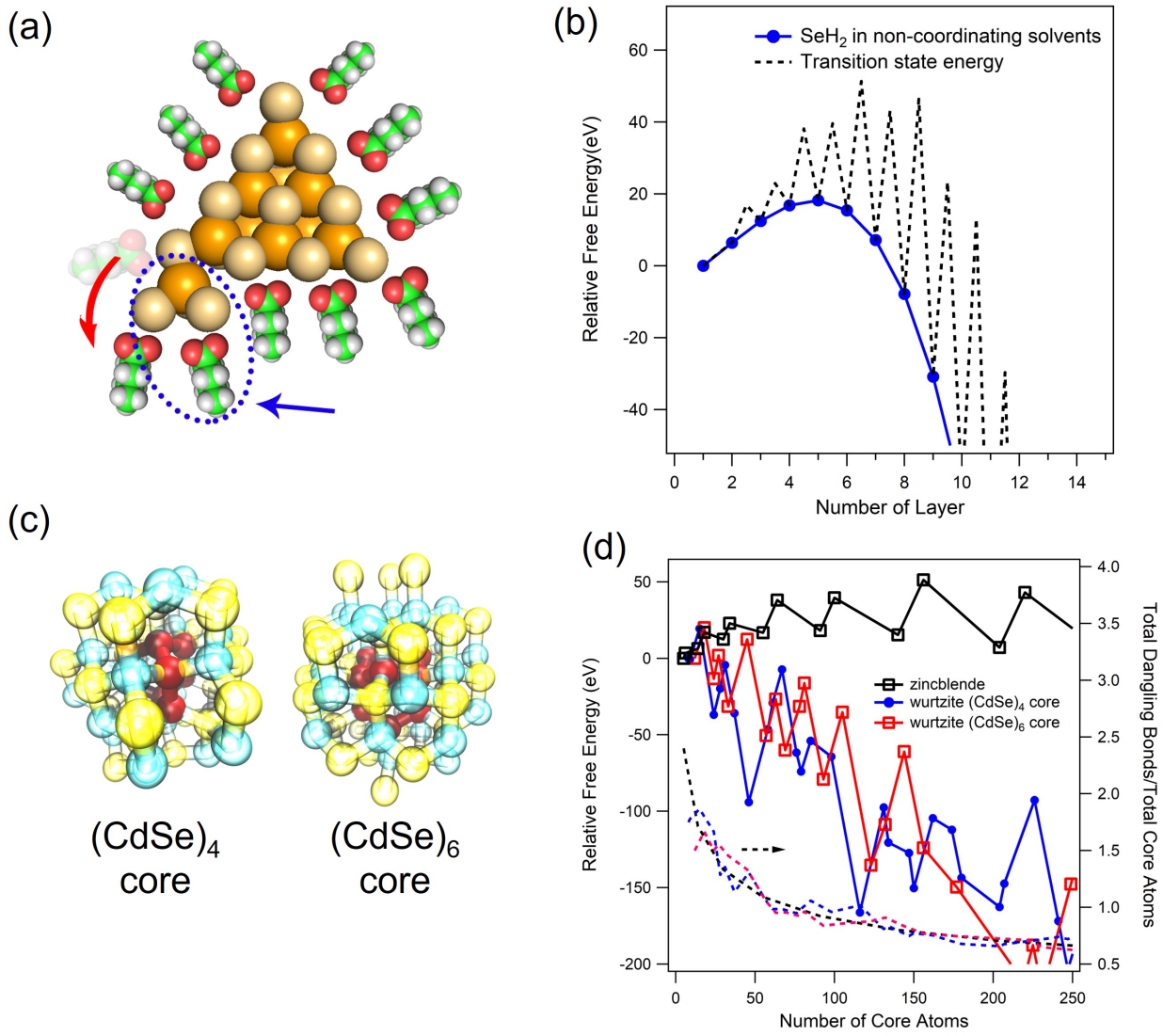

Figure 4: (a) Transition state structure of tetrahedral CdSe with addition of triangular adlayers. (b) corresponding free energy landscape of the thermodynamically stable structures and transition states in (a). (c) Wurtzite CdSe core structures generated stepwise based on the $(CdSe)_4$ adamantane cage and $(CdSe)_6$ cage (blue) respectively. The ligands are omitted for clarity. (d) Free energy landscapes for the cases in (c) as a function of total number of Cd and Se atoms. The dashed lines represent the ratio between total dangling bonds and total core atoms. The dashed arrow suggests that dashed curves follow the right axis.

$$\begin{aligned}
&\mathrm{Cd}_{\frac{(n+1)(n+2)(n+3)}{6}}\mathrm{Se}_{\frac{n(n+1)(n+2)}{6}}X_{(n+1)(n+2)}+\\
&\frac{(\mathrm{int}(n/2)+1)(\mathrm{int}(n/2)+2)}{2}\mathrm{CdX_2}+\frac{\mathrm{int}(n/2)(\mathrm{int}(n/2)+1)}{2}\mathrm{SeH_2}\Longrightarrow\\
&\mathrm{Cd}_{\frac{(n+1)(n+2)(n+3)}{6}+\frac{(\mathrm{int}(n/2)+1)(\mathrm{int}(n/2)+2)}{2}}\mathrm{Se}_{\frac{n(n+1)(n+2)}{6}+\frac{\mathrm{int}(n/2)(\mathrm{int}(n/2)+1)}{2}}X_{(n+1)(n+2)+2(\mathrm{int}(n/2)+1)}+\\
&\mathrm{int}(n/2)(\mathrm{int}(n/2)+1)\mathrm{HX}
\end{aligned} \tag{11}$$

This procedure requires the introduction of a number of Se atoms identical to those present in the current layer, along with the number of Cd atoms matching the count within the current layer. By meticulously assessing the alteration in the stoichiometry of the surface ligands, the associated driving force can be articulated as follows

$$\begin{aligned}
\Delta\Delta G^{\ddagger}(n) =&\frac{\mathrm{int}(n/2)(\mathrm{int}(n/2)+1)}{2}\epsilon^{\mathcal{P}}_{Cd-Se}+2\left(\mathrm{int}(n/2)+1\right)\epsilon^{\mathcal{P}}_{Cd-O}+\mathrm{int}(n/2)(\mathrm{int}(n/2)+1)\epsilon^{\mathcal{P}}_{O-H}\\
&-\left(\mathrm{int}(n/2)(\mathrm{int}(n/2)+1)\epsilon^{\mathcal{R}}_{Se-H}+\frac{(\mathrm{int}(n/2)+1)(\mathrm{int}(n/2)+2)}{2}\times 4\epsilon^{\mathcal{R}}_{Cd-O}\right)
\end{aligned} \tag{12}$$

Figure 4 (b) and Figure S.2 illustrate the variations in TS energy for the different pathways. The energy associated with adding an entire Se layer substantially escalates at each step. Consequently, if the reaction proceeds along this trajectory, the resultant reaction barrier would render it nearly impossible. This, in turn, would lead to the formation of a new energy landscape for the TS, yielding critical nuclei sizes distinct from those in the thermodynamic scenario. In contrast, when the reaction adheres to the "small-triangle" approach, it generates only relatively modest barriers, indicating that the growth of tetrahedral CdSe tends to favor the addition of these fragments rather than a "SILAR style" approach, whereby the cluster grows by successive formation of an entire Se layer followed by another Cd layer.

Remarkably, when traversing the "small-triangle" pathway, the energy barrier before

reaching the critical nucleus is higher than that encountered when following the two, nearby, thermodynamically stable structures. This suggests that even before the energy reaches the critical nucleus, there is a chance to trap the growth in specific metastable states, which is one of the factors contributing to the formation of "magic-sized" clusters. Once the critical nucleus is marginally exceeded, the TS barrier prompts the growth of the nanocrystal in discrete steps. This suggests that even for relatively large sizes, the tetrahedral nanocrystal may retain its "magic layer" characteristics instead of growing continuously. However, as the size increases sufficiently, there is a notable decrease in thermodynamic free energy, and the specifics of the TS become less crucial. So the reaction proceeds with continuous growth. It is important to emphasize that as we approach the large size limit, the transition state will closely resemble the subsequent stable structures of larger size for the choice of this transition state. Therefore, it becomes imperative to select a more suitable transition state for a more accurate depiction of the kinetic process. Nevertheless, our current study offers valuable insights into this matter.

Crystal Structure Effect

Analyzing the crystal structure poses a formidable challenge, necessitating the identification of an appropriate descriptor to clarify the fundamental distinctions between structures like zincblende and wurtzite. Unfortunately, the wurtzite structure lacks a clear bond-structure relationship, unlike the zincblende structure, and requires a numerical evaluation for all structures.

In Figure 4 (c), a method for generating wurtzite CdSe QDs is illustrated. The smallest unit, depicted in red, is the $(CdSe)_6$ or $(CdSe)_4$ structure, involving the formation of 15 Cd-Se bonds and 9 Cd dangling bonds for $(CdSe)_6$ and 9 Cd-Se bonds and 7 Cd dangling bonds for $(CdSe)_4$ respectively. Expanding from this $(CdSe)_6$ or $(CdSe)_4$ center, larger wurtzite structures are created with a stepwise increase in radius. The Cd-Se bond numbers and dangling bonds for each structure are calculated based on the "four coordination number"

criterion. Figure 4 (d) displays the free energy calculated using equations 6 and 7 as a function of the total core atom numbers, and is compared to the zincblende results. Given the imperfect structure (i.e. not a perfect adamantane cage) for every generated wurtzite structure, some structures within this landscape function as TSs or metastable structures.

It is apparent that, akin to the zincblende case, the energy for wurtzite structures initially increases and then decreases after reaching a critical size. However, both the energy barrier and the critical nuclei size for wurtzite are smaller than those of zincblende structures, suggesting that wurtzite structures are more easily formed than zincblende when combining SeH_2 and $Cd(oleate)_2$ in non-coordinating solvents, as experimentally observed.[46] The relationship between the overall count of surface dangling bonds and the total number of CdSe atom numbers indicates a reduction in the free energy of formation with decreasing numbers of surface traps. Nevertheless, further exploration is necessary to comprehend the chemical conditions required for the complete formation of the wurtzite structure.

It is important to highlight that the discussions presented in this paper rely on thermodynamic estimations and do not provide information about the reaction rate or speed. The kinetic aspect is addressed separately through the supersaturation term. Moreover, the energy barrier estimation in this paper transforms the kinetic issue into a thermodynamic one by assessing the structural energy of the transition state. Notably, even under equilibrium conditions where supersaturation equals one, our model enables easy estimation of the possibility of nanoparticle formation without requiring an empirical supersaturation value.

Conclusion

In conclusion, our proposed model hinges on intricate molecular insights during the pre-nucleation stage, introducing novel definitions for supersaturation, reaction units, and driving forces. It is intriguing that the driving force can be segregated into an intrinsic free energy term alongside the kinetic supersaturation contribution. This approach enables us to treat

the nucleation process akin to a straightforward chemical reaction even without introducing an empirical supersaturation value. Therefore, it enhances the precision of nanoparticle investigation and provides a strategy for designing NC synthesis protocols. This framework demonstrates its adaptability in comprehending various chemical aspects including precursor reactivity, surface chemistry, stoichiometry, crystal structures, and transition states throughout the nanocrystal formation process.

Computational Methods

The bond energy holds significant importance in determining the free energy discussed within this paper. To accurately obtain this bond energy, a high-level coupled-cluster method with perturbative triplet excitation, CCSD(T), utilizing the balanced polarized triple-ζ basis set (def2-TZVP),[47] is employed. CCSD(T) with a complete basis set is widely regarded as the "gold standard" in quantum chemistry research,[48] having demonstrated high accuracy in estimating both bond and reaction energies.[49,50] To mitigate computational expense, the domain-based local pair natural orbital coupled-cluster method (DLPNO-CCSD(T)) is additionally utilized.[35] Auxiliary Hellweg RI-MP2 (C) auxiliary basis set (def2-TZVP/C) and Weigend JK auxiliary basis set (def2/JK) are applied for this purpose.[51,52] Unrestricted Hartree-Fock (UHF) is used for all initial and final state energies if the bond breaking creates fragments with open shell electrons. All bond energy calculations are conducted using the ORCA software package,[53] while geometry optimization is performed at the M06-2X/def2-TZVP DFT level.[54] It is crucial to acknowledge that the selection of an electronic structure method is a critical decision, and further discussion is available in the SI. For consistency, only one set of parameters will be employed throughout this study.

The bond energy is estimated using the bond formation (E_{BE}) energy, which is defined as follows:

$$E_{BE} = E(A|B) - E(A) - E(B). \tag{13}$$

Here, $E(A|B)$ represents the energy of the entire species after forming a chemical bond, while $E(A)$ and $E(B)$ denote the energies of the radical fragments A and B, respectively. Because our reference states consist of non-interacting species in well-dispersed, non-coordinating solvents, the solvation effects addressed in this paper are founded on coordinating behavior rather than carbon chain interaction; thus, all bond energies are computed in a vacuum. To minimize the basis set superposition error (BSSE), counterpoise correction is incorporated. The bond energies utilized in this paper are list in Table 2.

Table 2: Bond energies and their associated fragments for calculation obtained from DLPNO-CCSD(T)/def2-TZVP level calculations.

Bond type	A	B	Bond Energy (eV)
$\epsilon^{\mathcal{R}}_{Cd-O}$	$CH_3CO_2\cdot$	$CH_3CO_2Cd\cdot$	-2.00
$\epsilon^{\mathcal{R}}_{Cd-N}$	$Cd(CH_3CO_2)_2(CH_3NH_2)$	CH_3NH_2	-0.78
$\epsilon^{\mathcal{R}}_{Se-H}$ (in SeH_2)	Se	H·	-4.04
$\epsilon^{\mathcal{R}}_{Se-H}$ (in RSeH)	$CH_3Se\cdot$	H·	-3.43
$\epsilon^{\mathcal{R}}_{Se-C}$	$CH_3C(\cdot)$=O	$CH_3C(=O)Se\cdot$	-2.37
$\epsilon^{\mathcal{R}}_{Se=P}$ (in R_2HP=Se)	$(CH_3)_2HP$:	Se	-3.99
$\epsilon^{\mathcal{R}}_{Se=P}$ (in TOP=Se)	$(CH_3)_3P$:	Se	-4.21
$\epsilon^{\mathcal{R}}_{H-P}$	$(CH_3)_2P(\cdot)$=Se	H·	-3.46
$\epsilon^{\mathcal{R}}_{C-P}$	$(CH_2)_2P(\cdot)$=Se	$CH_3\cdot$	-3.56
$\epsilon^{\mathcal{R}}_{Si-Se}$	$(CH_3)_3Si\cdot$	$(CH_3)_3SiSe\cdot$	-3.57
$\epsilon^{\mathcal{P}}_{Cd-O}$	$Cd_4Se(CH_3CO_2)_5(CH_3NH_2)_6\cdot$	$CH_3CO_2\cdot$	-2.30
$\epsilon^{\mathcal{P}}_{Cd-N}$	$Cd_4Se(CH_3CO_2)_6(CH_3NH_2)_5$	CH_3NH_2	-0.87
$\epsilon^{\mathcal{P}}_{Cd-N}$	$(CdSe)_{12}(CH_3NH_2)$	CH_3NH_2	-0.83
$\epsilon^{\mathcal{P}}_{Cd-Se}$	$(CdSe)_{13}$	Cd and Se	-1.66
$\epsilon^{\mathcal{P}}_{O-H}$	$CH_3CO_2\cdot$	H·	-5.35
$\epsilon^{\mathcal{P}}_{O-C}$ (in R_2HP=Se)	$CH_3C(\cdot)$=O	$CH_3CO_2\cdot$	-4.06
$\epsilon^{\mathcal{P}}_{O-C}$ (in TOP=Se)	$CH_3CO_2\cdot$	$CH_3\cdot$	-4.30
$\epsilon^{\mathcal{P}}_{O-P}$	$CH_3CO_2\cdot$	$(CH_3)_2P\cdot$	-3.70
$\epsilon^{\mathcal{P}}_{Si-O}$	$(CH_3)_3Si\cdot$	$(CH_3)_2CO_2\cdot$	-5.48
$\epsilon^{\mathcal{P}}_{Se-Se}$	$CH_3Se\cdot$	$CH_3Se\cdot$	-2.26

Supporting Information

The supporting information includes more computational details, the discussion of spontaneous nucleation conditions, the effect of choosing different bond energies and different

transition state pathways.

Acknowledgments

The authors thank the ARC for support through ARC Grant CE170100026. Z.C. thanks the Australian Government and the University of Melbourne for a Research Training Program (RTP) Scholarship, and thanks Dr. Anjay Manian for useful discussions. This work was also supported by computational resources provided by the Australian Government through the National Computational Infrastructure, National Facility and the Pawsey Supercomputer Centre.

References

(1) Mullin, J. In *Crystallization (Fourth Edition)*, fourth edition ed.; Mullin, J., Ed.; Butterworth-Heinemann: Oxford, 2001; pp 181–215.

(2) Xie, R.; Li, Z.; Peng, X. Nucleation Kinetics vs Chemical Kinetics in the Initial Formation of Semiconductor Nanocrystals. *J. Am. Chem. Soc.* **2009**, *131*, 15457–15466.

(3) Oxtoby, D. W. Nucleation of First-Order Phase Transitions. *Acc. Chem. Res.* **1998**, *31*, 91–97.

(4) Yu, K. CdSe Magic-Sized Nuclei, Magic-Sized Nanoclusters and Regular Nanocrystals: Monomer Effects on Nucleation and Growth. *Adv. Mater.* **2012**, *24*, 1123–1132.

(5) Thanh, N. T. K.; Maclean, N.; Mahiddine, S. Mechanisms of Nucleation and Growth of Nanoparticles in Solution. *Chem. Rev.* **2014**, *114*, 7610–7630, PMID: 25003956.

(6) Karthika, S.; Radhakrishnan, T. K.; Kalaichelvi, P. A Review of Classical and Nonclassical Nucleation Theories. *Crystal Growth & Design* **2016**, *16*, 6663–6681.

(7) Whitehead, C. B.; Özkar, S.; Finke, R. G. LaMer's 1950 model of particle formation: a review and critical analysis of its classical nucleation and fluctuation theory basis, of competing models and mechanisms for phase-changes and particle formation, and then of its application to silver halide, semiconductor, metal, and metal-oxide nanoparticles. *Mater. Adv.* **2021**, *2*, 186–235.

(8) Becker, R.; Döring, W. Kinetische Behandlung der Keimbildung in übersättigten Dämpfen. *Annalen der Physik* **1935**, *416*, 719–752.

(9) LaMer, V. K.; Dinegar, R. H. Theory, Production and Mechanism of Formation of Monodispersed Hydrosols. *J. Am. Chem. Soc.* **1950**, *72*, 4847–4854.

(10) Ostwald, W. Über die vermeintliche Isomerie des roten und gelben Quecksilberoxyds und die Oberflächenspannung fester Körper. *Zeitschrift für Physikalische Chemie* **1900**, *34U*, 495–503.

(11) Mer, V. K. L. Nucleation in Phase Transitions. *Industrial & Engineering Chemistry* **1952**, *44*, 1270–1277.

(12) Reiss, H.; Katz, J. L.; Cohen, E. R. Translation–Rotation Paradox in the Theory of Nucleation. *J. Chem. Phys.* **1968**, *48*, 5553–5560.

(13) Reiss, H. The Growth of Uniform Colloidal Dispersions. *J. Chem. Phys.* **2004**, *19*, 482–487.

(14) Lifshitz, I.; Slyozov, V. The kinetics of precipitation from supersaturated solid solutions. *J. Phys. Chem. Solids* **1961**, *19*, 35–50.

(15) Wagner, C. Ostwald ripening theory. *Ber Bunsenges Phys Chem* **1961**, *65*, 581–591.

(16) Finney, E. E.; Finke, R. G. Nanocluster nucleation and growth kinetic and mechanistic studies: A review emphasizing transition-metal nanoclusters. *J. Colloid Interface Sci.* **2008**, *317*, 351–374.

(17) Iland, K.; Wölk, J.; Strey, R.; Kashchiev, D. Argon nucleation in a cryogenic nucleation pulse chamber. *J. Chem. Phys.* **2007**, *127*, 154506.

(18) Sinha, S.; Laksmono, H.; Wyslouzil, B. E. A cryogenic supersonic nozzle apparatus to study homogeneous nucleation of Ar and other simple molecules. *Rev. Sci. Instrum.* **2008**, *79*, 114101.

(19) Sinha, S.; Bhabhe, A.; Laksmono, H.; Wölk, J.; Strey, R.; Wyslouzil, B. Argon nucleation in a cryogenic supersonic nozzle. *J. Chem. Phys.* **2010**, *132*, 064304.

(20) Lee, J.; Yang, J.; Kwon, S. G.; Hyeon, T. Nonclassical nucleation and growth of inorganic nanoparticles. *Nat. Rev. Mater.* **2016**, *1*.

(21) Yoreo, J. J. D.; Gilbert, P. U. P. A.; Sommerdijk, N. A. J. M.; Penn, R. L.; Whitelam, S.; Joester, D.; Zhang, H.; Rimer, J. D.; Navrotsky, A.; Banfield, J. F.; Wallace, A. F.; Michel, F. M.; Meldrum, F. C.; Cölfen, H.; Dove, P. M. Crystallization by particle attachment in synthetic, biogenic, and geologic environments. *Science* **2015**, *349*, aaa6760.

(22) Girshick, S. L.; Chiu, C. Kinetic nucleation theory: A new expression for the rate of homogeneous nucleation from an ideal supersaturated vapor. *J. Chem. Phys.* **1990**, *93*, 1273–1277.

(23) Wang, T.; Wang, Z.; Wang, S.; Chen, X.; Luan, C.; Yu, K. Thermally-Induced Isomerization of Prenucleation Clusters During the Prenucleation Stage of CdTe Quantum Dots. *Angew. Chem. Int. Ed.* **2023**, *62*, e202310234.

(24) Cahn, J. W. On spinodal decomposition. *Acta Metallurgica* **1961**, *9*, 795–801.

(25) Katz, J. L.; Wiedersich, H. Nucleation theory without Maxwell Demons. *J. Colloid Interface Sci.* **1977**, *61*, 351–355.

(26) Du, H.; Nadykto, A. B.; Yu, F. Quantum-mechanical solution to fundamental problems of classical theory of water vapor nucleation. *Phys. Rev. E* **2009**, *79*, 021604.

(27) Steckel, J. S.; Yen, B. K. H.; Oertel, D. C.; Bawendi, M. G. On the Mechanism of Lead Chalcogenide Nanocrystal Formation. *J. Am. Chem. Soc.* **2006**, *128*, 13032–13033.

(28) Yu, K.; Liu, X.; Qi, T.; Yang, H.; Whitfield, D. M.; Q, Y. C.; Huisman, E. J.; Hu, C. General low-temperature reaction pathway from precursors to monomers before nucleation of compound semiconductor nanocrystals. *Nat. Commun.* **2016**, *7*, 12223.

(29) Pun, A. B.; Mazzotti, S.; Mule, A. S.; Norris, D. J. Understanding Discrete Growth in Semiconductor Nanocrystals: Nanoplatelets and Magic-Sized Clusters. *Acc. Chem. Res.* **2021**, *54*, 1545–1554.

(30) Mule, A. S.; Mazzotti, S.; Rossinelli, A. A.; Aellen, M.; Prins, P. T.; van der Bok, J. C.; Solari, S. F.; Glauser, Y. M.; Kumar, P. V.; Riedinger, A.; Norris, D. J. Unraveling the Growth Mechanism of Magic-Sized Semiconductor Nanocrystals. *J. Am. Chem. Soc.* **2021**, *143*, 2037–2048.

(31) Kiet A., N.; Ruth, P.; Paul N., D. Systematic Study of Structure, Stability, and Electronic Absorption of Tetrahedral CdSe Clusters with Carboxylate and Amine Ligands. *J. Phys. Chem. A* **2018**, *122*, 6704–6712.

(32) Beecher, A. N.; Yang, X.; Palmer, J. H.; LaGrassa, A. L.; Juhas, P.; Billinge, S. J. L.; Owen, J. S. Atomic Structures and Gram Scale Synthesis of Three Tetrahedral Quantum Dots. *J. Am. Chem. Soc.* **2014**, *136*, 10645–10653.

(33) Chen, Z.; Beimborn, J. C. I.; Kirkwood, N.; Russo, S. P.; Weber, J. M.; Mulvaney, P. Size-Dependent Response of CdSe Quantum Dots to Hydrostatic Pressure. *J. Phys. Chem. C* **2023**, *127*, 8657–8669.

(34) Weatherspoon, H.; Peters, B. Broken bond models, magic-sized clusters, and nucleation theory in nanoparticle synthesis. *J. Chem. Phys.* **2023**, *158*, 114306.

(35) Riplinger, C.; Sandhoefer, B.; Hansen, A.; Neese, F. Natural triple excitations in local coupled cluster calculations with pair natural orbitals. *J. Chem. Phys.* **2013**, *139*, Cited by: 1203.

(36) Čapek, R. K.; Lambert, K.; Dorfs, D.; Smet, P. F.; Poelman, D.; Eychmüller, A.; Hens, Z. Synthesis of Extremely Small CdSe and Bright Blue Luminescent CdSe/ZnS Nanoparticles by a Prefocused Hot-Injection Approach. *Chemistry of Materials* **2009**, *21*, 1743–1749.

(37) Liu, H.; Owen, J. S.; Alivisatos, A. P. Mechanistic Study of Precursor Evolution in Colloidal Group II-VI Semiconductor Nanocrystal Synthesis. *J. Am. Chem. Soc.* **2007**, *129*, 305–312.

(38) Cossairt, B. M.; Owen, J. S. CdSe Clusters: At the Interface of Small Molecules and Quantum Dots. *Chemistry of Materials* **2011**, *23*, 3114–3119.

(39) Riedinger, A.; Mule, A. S.; Knüsel, P. N.; Ott, F. D.; Rossinelli, A. A.; Norris, D. J. Identifying reactive organo-selenium precursors in the synthesis of CdSe nanoplatelets. *Chem. Commun.* **2018**, *54*, 11789–11792.

(40) Jasieniak, J.; Mulvaney, P. From Cd-Rich to Se-Rich - the Manipulation of CdSe Nanocrystal Surface Stoichiometry. *J. Am. Chem. Soc.* **2007**, *129*, 2841–2848.

(41) Gao, Y.; Peng, X. Photogenerated Excitons in Plain Core CdSe Nanocrystals with Unity Radiative Decay in Single Channel: The Effects of Surface and Ligands. *J. Am. Chem. Soc.* **2015**, *137*, 4230–4235.

(42) Dance, I. G.; Choy, A.; Scudder, M. L. Syntheses, properties, and molecular and crystal structures of (Me4N)4[E4M10(SPh)16] (E = sulfur or selenium; M = zinc or cadmium):

molecular supertetrahedral fragments of the cubic metal chalcogenide lattice. *J. Am. Chem. Soc.* **1984**, *106*, 6285–6295.

(43) Wang, Y.; Liu, Y.-H.; Zhang, Y.; Wang, F.; Kowalski, P. J.; Rohrs, H. W.; Loomis, R. A.; Gross, M. L.; Buhro, W. E. Isolation of the Magic-Size CdSe Nanoclusters [(CdSe)13(n-octylamine)13] and [(CdSe)13(oleylamine)13]. *Angew. Chem. Int. Ed.* **2012**, *51*, 6154–6157.

(44) Sanville, E.; Burnin, A.; BelBruno, J. J. Experimental and Computational Study of Small (n = 1-16) Stoichiometric Zinc and Cadmium Chalcogenide Clusters. *J. Phys. Chem. A* **2006**, *110*, 2378–2386.

(45) Nguyen, K. A.; Day, P. N.; Pachter, R. Understanding Structural and Optical Properties of Nanoscale CdSe Magic-Size Quantum Dots: Insight from Computational Prediction. *J. Phys. Chem. C* **2010**, *114*, 16197–16209.

(46) Murray, C. B.; Norris, D. J.; Bawendi, M. G. Synthesis and characterization of nearly monodisperse CdE (E = sulfur, selenium, tellurium) semiconductor nanocrystallites. *J. Am. Chem. Soc.* **1993**, *115*, 8706–8715.

(47) Weigend, F.; Ahlrichs, R. Balanced basis sets of split valence, triple zeta valence and quadruple zeta valence quality for H to Rn: Design and assessment of accuracy. *Phys. Chem. Chem. Phys.* **2005**, *7*, 3297–3305.

(48) Klopper, W.; Noga, J.; Koch, H.; Helgaker, T. Multiple basis sets in calculations of triples corrections in coupled-cluster theory. *Theor. Chem. Acc.* **1997**, *97*, 164 – 176.

(49) Black, J. A.; Knowles, P. J. Statistical analysis of activation and reaction energies with quasi-variational coupled-cluster theory. *Mol. Phys.* **2018**, *116*, 1421–1427.

(50) Zhang, J.; Valeev, E. F. Prediction of Reaction Barriers and Thermochemical Properties

with Explicitly Correlated Coupled-Cluster Methods: A Basis Set Assessment. *J. Chem. Theory Comput.* **2012**, *8*, 3175–3186.

(51) Hellweg, A.; Hättig, C.; Höfener, S.; Klopper, W. Optimized accurate auxiliary basis sets for RI-MP2 and RI-CC2 calculations for the atoms Rb to Rn. *Theor. Chem. Acc.* **2007**, *117*, 587–597.

(52) Weigend, F. Hartree–Fock exchange fitting basis sets for H to Rn †. *J. Comput. Chem.* **2008**, *29*, 167–175.

(53) Neese, F.; Wennmohs, F.; Becker, U.; Riplinger, C. The ORCA quantum chemistry program package. *J. Chem. Phys.* **2020**, *152*, 224108.

(54) Zhao, Y.; Truhlar, D. G. The M06 suite of density functionals for main group thermochemistry, thermochemical kinetics, noncovalent interactions, excited states, and transition elements: two new functionals and systematic testing of four M06-class functionals and 12 other functionals. *Theor. Chem. Acc.* **2008**, *120*, 215–241.

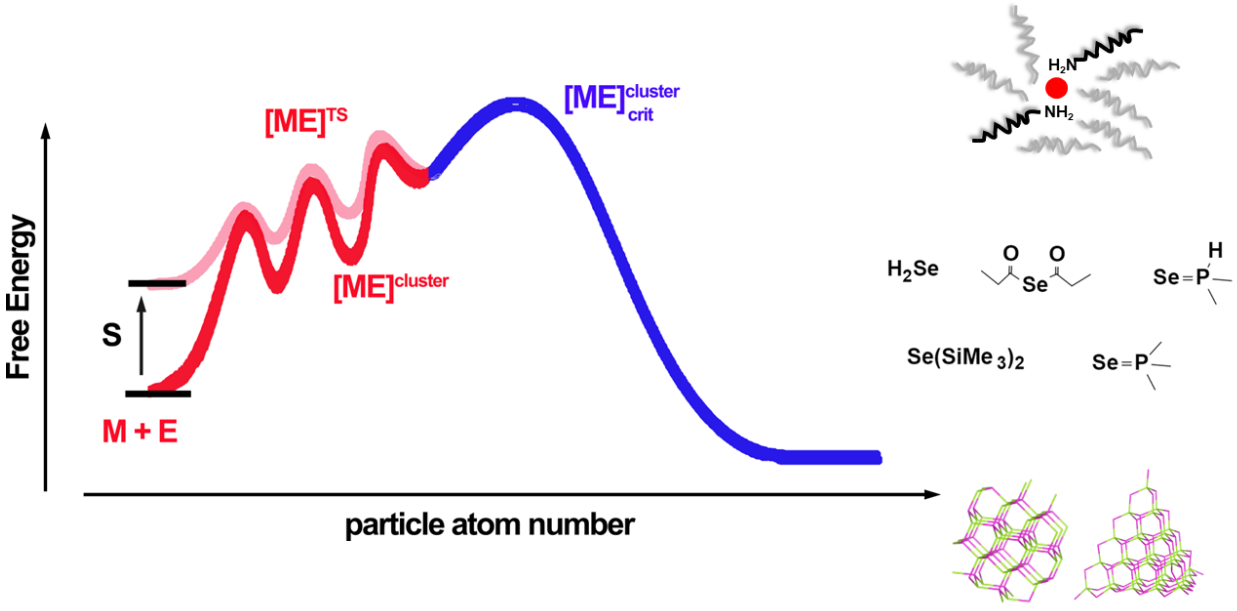

Figure 5: Proposed TOC